Neuron, Vol. 19, 697–709, September, 1997, Copyright ©1997 by Cell Press

# Differences in Synaptic $GABA_A$ Receptor Number Underlie Variation in GABA Mini Amplitude

**Zoltan Nusser,*† Stuart Cull-Candy,* and Mark Farrant***
*Department of Pharmacology
University College London
London WC1E 6BT
United Kingdom
†Medical Research Council
Anatomical Neuropharmacology Unit
University of Oxford
Oxford OX1 3TH
United Kingdom

## Summary

**In many neurons, responses to individual quanta of transmitter exhibit large variations in amplitude. The origin of this variability, although central to our understanding of synaptic transmission and plasticity, remains controversial. To examine the relationship between quantal amplitude and postsynaptic receptor number, we adopted a novel approach, combining patch-clamp recording of synaptic currents with quantitative immunogold localization of synaptic receptors. Here, we report that in cerebellar stellate cells, where variability in GABA miniature synaptic currents is particularly marked, the distribution of quantal amplitudes parallels that of synaptic $GABA_A$ receptor number. We also show that postsynaptic $GABA_A$ receptor density is uniform, allowing synaptic area to be used as a measure of relative receptor content. Flurazepam, which increases $GABA_A$ receptor affinity, prolongs the decay of all miniature currents but selectively increases the amplitude of large events. From this differential effect, we show that a quantum of GABA saturates postsynaptic receptors when $<$80 receptors are present but results in incomplete occupancy at larger synapses.**

## Introduction

The manner in which groups of neurons process information is governed, to a large extent, by the behavior of their synaptic connections. Factors that determine this behavior include the number of transmitter release sites, the probability of transmitter release at each site, and the size of the postsynaptic response generated at each connection. Traditionally, these parameters have been estimated by analysing the fluctuations in the amplitude of postsynaptic responses, a method first applied at the neuromuscular junction (del Castillo and Katz, 1954). Here, the amplitudes of miniature end-plate potentials, produced by individual packets of transmitter, have a Gaussian distribution with a mean value equal to the size of the quantal event underlying the evoked responses (del Castillo and Katz, 1954). By contrast, in most central neurons, distributions of the amplitude of miniature excitatory and inhibitory postsynaptic responses cannot be described by a Gaussian but are skewed toward larger values, raising the question of what determines the size of the quantal event and complicating the interpretation of quantal analysis (Jack et al., 1994; Edwards, 1995; Walmsley, 1995; Frerking and Wilson, 1996a). Variation in the size of miniature postsynaptic responses may arise from mechanisms intrinsic to single release sites (Bekkers et al., 1990; Gulyas et al., 1993; Tong and Jahr, 1994b; Bekkers and Stevens, 1995; Liu and Tsien, 1995; Frerking et al., 1995; Silver et al., 1996), differences between sites (Edwards et al., 1990; Otis and Mody, 1992; De Konink and Mody, 1994; Tong and Jahr, 1994a; Borst et al., 1994; Poncer et al., 1996), or a combination of both. Establishing the causes of such variation is essential to our understanding of the basic mechanisms of normal synaptic transmission and the ways in which plastic changes in synaptic efficacy may arise.

In the case of miniature inhibitory postsynaptic currents (mIPSCs) at central synapses, several mechanisms have been proposed to account for the wide variability in their amplitude. These include the possibility of multiquantal transmitter release (Ropert et al., 1990), variation in transmitter content of different vesicles (Frerking et al., 1995), the stochastic behavior of channel gating (Faber et al., 1992), or differences in postsynaptic receptor number at different sites (Edwards et al., 1990; De Koninck and Mody, 1994; Borst et al., 1994). A method that enables possible variability in postsynaptic receptor number to be examined directly is the electron microscopic immunogold labeling of neurotransmitter receptor subunits (Triller et al., 1985; Nusser et al., 1994, 1995a; Matsubara et al., 1996; Popratiloff et al., 1996). Here, we have used this technique, together with whole-cell voltage-clamp recording, in order to investigate the mechanisms underlying the variability in the amplitude of $GABA_A$ receptor-mediated mIPSCs in cerebellar stellate cells (Llano and Gerschenfeld, 1993). Stellate cells were chosen for this approach as they express only the $\alpha$1, $\beta$2, and $\gamma$2 subunits of the $GABA_A$ receptor (Persohn et al., 1992; Somogyi et al., 1996) and, given the preferential coassembly of these subunits, are expected to express only a single type of $GABA_A$ receptor (Angelotti and Macdonald, 1993; Tretter et al., 1997). Thus, any one of these subunits can be used as a target for immunolabeling, variability of which should reflect the variability in total receptor number. Furthermore, the dendritic arborization of these cells is not very extensive, allowing good voltage control of the synapses (Llano and Gerschenfeld, 1993). Our results suggest that the major contribution to the variability in the amplitude of mIPSCs at these synapses is variation in postsynaptic $GABA_A$ receptor number, and that on a single cell there may be synapses that function differently depending on their size and the number of postsynaptic receptors present.

## Results

### Properties of Miniature IPSCs

Voltage-clamp recordings were made from a total of 40 stellate cells in cerebellar slices from rats aged between

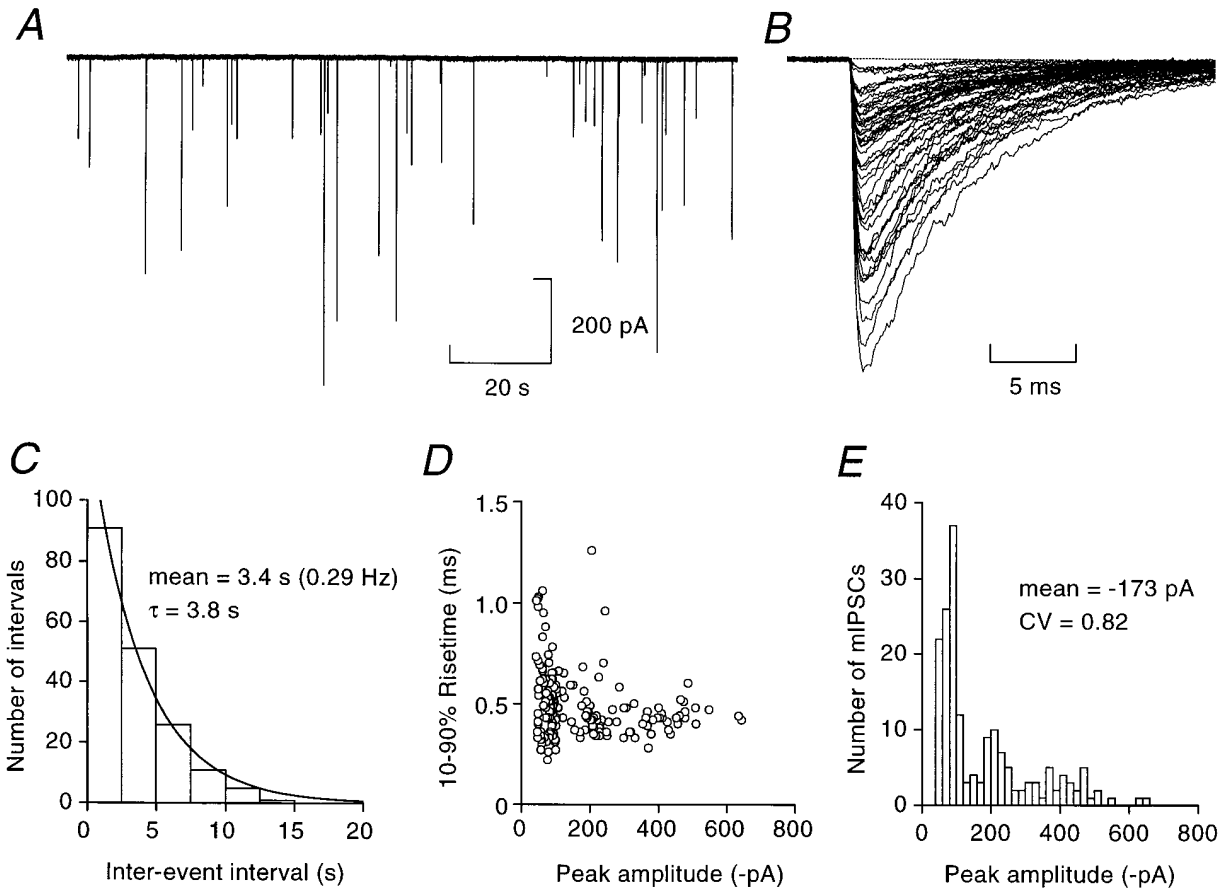


Figure 1. mIPSCs Occur Randomly and Exhibit a Wide Range of Amplitudes

(A and B) Whole-cell voltage clamp records from a stellate cell (P21) held at −70 mV, showing spontaneous inward currents (mIPSCs) during perfusion with an extracellular solution containing 5μM CNQX, 10 μM D-AP5, 0.3 μM strychnine, and 0.5 μM TTX.

(A) Continuous record illustrating the low frequency of mIPSCs, 0.22 Hz in this cell, and their widely differing amplitudes. For display, currents were filtered at 1 kHz and digitized at 2 kHz.

(B) Fifty consecutive mIPSCs superimposed and aligned on their rising phase (same current scale as in [A]). Note their rapid rise and large amplitude range (28–692 pA). The dotted line indicates the pre-event baseline current. Currents were filtered at 4 kHz and digitized at 20 kHz.

(C) Histogram of interevent intervals for mIPSCs recorded from another cell (P18) under the same conditions as in (A) and (B). The data are well described by an exponential function (smooth curve) with a time constant close to the mean frequency, indicating the random occurrence of mIPSCs.

(D) Scatter plot of rise time versus peak amplitude (same cell as in [C]). Note the lack of a linear relationship between these parameters.

(E) Amplitude histogram of mIPSCs recorded from the same cell as in (C) (n = 176). The distribution is not Gaussian but is skewed toward larger values.

13 and 26 days (P13–P26). Spontaneously occurring inward currents were observed in all cells, and these were completely blocked by the $GABA_A$ receptor antagonist bicuculline methobromide (10 μM). The frequency of IPSCs was greatly reduced in the presence of tetrodotoxin (TTX, 0.5 μM), indicating that most were action potential dependent. TTX-resistant mIPSCs were recorded in all cells; the measured parameters of these currents showed no consistent developmental change in cells from animals older than P16, and only data from cells in this group (P18–P26; mean, P23; n = 12) were included in the present study. The mIPSCs occurred relatively infrequently (Figure 1A; 0.19 ± 0.26 Hz, mean ± SD), and the interevent intervals were distributed randomly (Figure 1C). The currents had a rapid rise time (10%–90%; 417 ± 43 μs; Figure 1B), with no evidence of inflections on the rising phase. Together, these data suggest that the currents represent discrete responses to individual quanta of transmitter (see also Llano and Gerschenfeld, 1993). The mean amplitude of these quantal events was 198.9 ± 64.2 pA, and the decay time course of the averaged currents was best fitted by two exponential components (time constants, 6.4 ± 1.7 ms and 25.5 ± 10.6 ms; data not shown), with the fast component contributing 84.8% ± 5.0% to the peak amplitude.

**Distributions of mIPSC Amplitudes**

In each cell, the amplitude of mIPSCs varied enormously, from a few tens of pA to several hundred pA (Figures 1A and 1B). The amplitudes of the individual smallest and largest mIPSCs in each cell were 22.4 ± 8.2 pA (range, 11.8–39.2) and 548.7 ± 188.7 pA (range, 201.5–827.4), respectively. The average coefficient of variation (CV; SD/mean) of the amplitudes was 0.61 ±

0.17 (range, 0.4–0.9). In 10 out of 12 cases, the amplitude distributions were skewed toward larger amplitudes and differed significantly from a Gaussian distribution ($p < 0.05$, Shapiro-Wilk test). Although there was no linear correlation between the rise time and the peak amplitude (Figure 1D), in most cells the variability in the rise time of small mIPSCs was greater than that of larger mIPSCs. This is likely to result from stochastic channel properties rather than dendritic filtering (Bier et al., 1996); indeed, the fast rise times of mIPSCs in stellate cells are comparable to those seen in other electrotonically compact cells, such as cerebellar granule cells (Brickley et al., 1996) and pituitary melanotropes (Borst et al., 1994).

### Variability of Synaptic $GABA_A$ Receptor Content Determined by Immunogold Labeling

To examine whether differences in $GABA_A$ receptor content between synapses could account for the variability in the amplitude of mIPSC in stellate cells, we labeled receptors using subunit-specific antibodies and quantified their distribution at the electron microscopic level using an immunogold method (Nusser et al., 1994, 1995a). We examined immunolabeling in symmetrical synapses on interneuron dendrites in the outer two-thirds of the molecular layer of the cerebellum; Golgi and basket cell dendrites are also present in the molecular layer, but in this region the majority of interneuron dendrites are expected to belong to stellate cells (Palay and Chan-Palay, 1974). Interneuron dendrites were identified by their convergent asymmetrical synaptic inputs directly onto the dendritic shaft and by the absence of cisternal stacks. The frequency of symmetrical synapses was approximately 10-fold less than that of asymmetrical synapses, and the distance between GABAergic synapses was relatively large, such that most of the time a maximum of one GABAergic synapse was present in a section of each dendrite. Immunolabeling with antibodies against the $\alpha$1 or $\beta$2/3 subunits of the $GABA_A$ receptor showed large differences in immunoparticle content between different symmetrical synapses; on a single ultrathin section, some synapses contained as few as 2–3 immunoparticles, whereas others contained >25 immunoparticles (Figure 2). Similar observations have also been made with antibodies against the $\gamma$2 subunit (Somogyi et al., 1996), consistent with the likely expression of a single type of receptor containing all three subunits.

To estimate the immunoreactive receptor content of the entire postsynaptic area, we serially sectioned the molecular layer and reacted each ultrathin section for the $\alpha$1 subunit (Figure 2). Immunoparticles were then counted within anatomically defined synaptic junctions throughout the serial sections. Using this approach, some reconstructed synapses were found to contain >180 immunoparticles (Figures 2A and 2B) and to pass through as many as 18 sections. However, the majority of synapses contained fewer immunoparticles (20–50) and were present on only 3–5 sections (Figure 2A). The distribution of the number of immunoparticles per synapse was not Gaussian ($p < 0.05$, Shapiro-Wilk test) but was skewed toward larger values (Figure 3A). The mean number of particles per synapse was 55.8 $\pm$ 44.9 (range, 6–184; CV = 0.81). Although synapses included in this analysis originated from several interneurons, the large differences in $GABA_A$ receptor number were clearly present in individual cells and thus were not due solely to differences between cells. In each case where more than one synaptic junction was identified on a single dendrite within the volume of tissue analyzed ($n = 3$), the immunoparticle content of these synapses varied over a roughly similar range to that seen in the population of synapses as a whole. As shown in Figures 2A and 3A, some synapses were found to contain up to 20 times as many particles as others on the same dendrite.

### Relationship between Size of Synapses and Their $GABA_A$ Receptor Content

A comparison of different synapses showed that large synapses contained more immunoparticles than small ones. A quantitative examination of all synapses revealed a positive, linear correlation between synaptic area and the number of gold particles per synapse, indicating a uniform receptor density across all synapses (Figure 3B). This linear correlation remained when the primary antibody concentration was halved (Figure 3B), indicating that uniformity of immunoparticle density was not due to a saturation of labeling. Given this correlation, the synaptic area itself can be used as a measure of the relative synaptic receptor content. We therefore reexamined the distribution of synaptic areas in osmium-treated, epoxy resin-embedded tissue, in which fine ultrastructural details are better defined than in Lowicryl resin-embedded tissue. Synapses between GABA immunopositive axon terminals and GABA positive interneuron dendrites or somata were reconstructed from serial sections, and their areas were measured. The distribution of synaptic areas was skewed toward larger values (Figure 3C; mean = 0.152 $\pm$ 0.099 $\mu m^2$; CV = 0.65), with a ~20-fold difference between the smallest (0.018 $\mu m^2$) and the largest (0.361 $\mu m^2$) synapse. As with immunoparticle number, this large variability in synaptic area was also observed between synapses converging onto individual cells (Figure 3C). Such variability and skewed distribution of synaptic areas has also been reported in other central neurons (see Pierce and Mendell, 1993; Sur et al., 1995; and references therein), and it is tempting to speculate that this may also indicate a corresponding variability in postsynaptic receptor number (see Walmsley, 1995). In our study, no consistent difference in the width of the synaptic cleft (~20 nm) could be detected between synapses; therefore, the 20-fold difference in synaptic areas implies an equivalent variation in the volume of the cleft.

### The Effect of Flurazepam on mIPSCs

The large variability in postsynaptic receptor number and cleft volume indicated by our results raises the possibility of differences in receptor occupancy, following the release of single quanta, at different sites on stellate cells. One way to assess the degree of receptor occupancy is through the use of pharmacological agents that increase the affinity of receptors for their ligands. In the case of synaptic $GABA_A$ receptors, this has been achieved using benzodiazepine agonists (Otis and

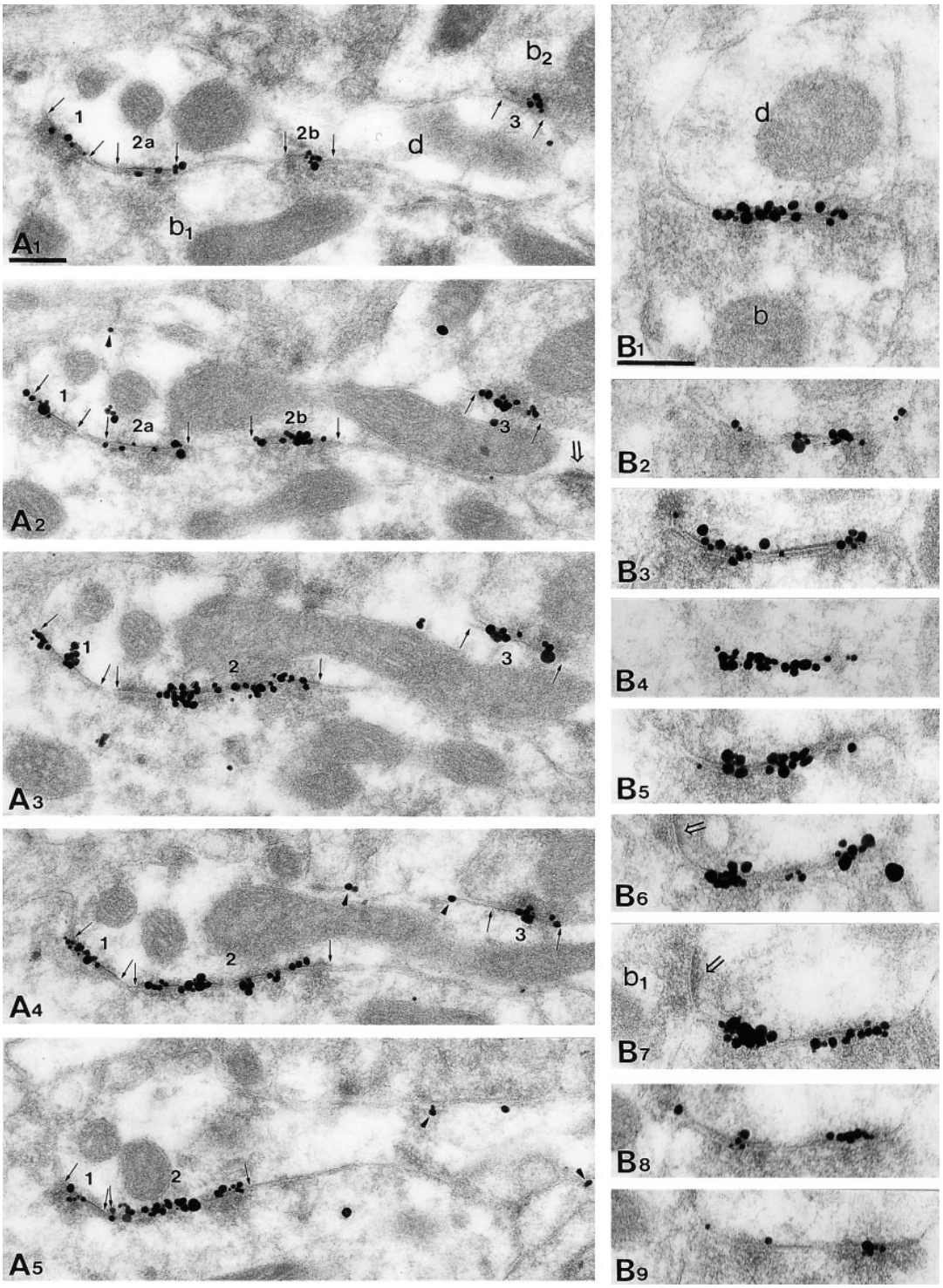


Figure 2. Electron Microscopic Demonstration of the Large Variability in the Number of Immunoreactive $\alpha$1 Subunits per Synapse

(A) Electron micrographs of serial sections ($A_1$–$A_5$) through Lowicryl resin-embedded rat cerebellar cortex showing postembedding immunogold labeling for the $\alpha$1 subunit of the $GABA_A$ receptor. Note the large variability in immunoparticle content of the three synaptic junctions (1–3, between the arrows) made by two axon terminals ($b_1$ and $b_2$) with an individual interneuron dendrite (d). On sections 1 and 2, four discrete synaptic specializations can be identified (1, 2a, 2b, and 3). However, from sections 3–5 it is apparent that 2a and 2b are part of the same perforated synapse. Silver intensified gold particles are enriched in the synaptic junctions, though extrasynaptic receptors (arrowheads) are also found at a lower density. The micrographs were chosen to illustrate the variability in particle content of different synapses on the same dendrite. In this case, the synapses were unusually close to each other and are thus not representative of the entire population, where no more than one GABAergic synapse was usually present in a section of each dendrite. The immunoparticle content of these synapses is indicated by the closed circles in Figure 3A. Synapses 1 and 2 extended beyond the sections illustrated (10 and 11 sections, respectively)

Mody, 1992; De Koninck and Mody, 1994; Frerking et al., 1995; Poncer et al., 1996). Benzodiazepine agonists increase the binding affinity of $GABA_A$ receptors for GABA (Rogers et al., 1994; Lavoie and Twyman, 1996) and would be expected to increase the amplitude of mIPSCs only if postsynaptic receptors are not fully occupied following the release of a packet of GABA.

In the presence of the benzodiazepine agonist flurazepam (3 $\mu$M), the decay times of averaged mIPSCs were prolonged (62% decay time, 7.7 $\pm$ 2.1 ms to 19.6 $\pm$ 4.6 ms; $p < 0.01$, Student's t test; $n = 5$), as seen at other synapses (Vicini et al., 1986; Otis and Mody, 1992; Zhang et al., 1993; De Koninck and Mody, 1994; Frerking et al., 1995; Poncer et al., 1996). Both the fast and slow time constants of decay were increased (105% and 91%, respectively), with a small (8%) reduction in the fractional contribution of the fast component. There was no significant change in rise time (control, 446 $\pm$ 48 $\mu$s; flurazepam, 453 $\pm$ 65 $\mu$s). In all five cells, the amplitude of the averaged mIPSCs was significantly increased in the presence of flurazepam (from 170.7 $\pm$ 41.1 pA to 245.1 $\pm$ 21.9 pA; $p < 0.05$, Student's t test). However, examination of amplitude histograms (Figure 4A) indicated that in four of these cells this increase resulted from a selective effect on the larger events, with the amplitude of smaller events apparently unaffected. This is better seen in cumulative distributions (Figure 4B), where the two distributions (control and flurazepam) overlap up to $\sim$140 pA, but deviate from each other at larger amplitudes.

There are two possible explanations for this result. On the one hand, receptors giving rise to "small" mIPSCs may be benzodiazepine insensitive, while the ones giving rise to "large" events may be benzodiazepine sensitive. Alternatively, receptors underlying both small and large mIPSCs may be benzodiazepine-sensitive, but flurazepam may have no effect on the amplitude of the small mIPSCs because the postsynaptic receptors are fully occupied following the release of a packet of GABA. To test these possibilities, we grouped mIPSCs according to their amplitudes; the first group contained currents smaller than an arbitrary cut-off value of $\sim$140 pA (arrow in Figure 4A), and the second group contained larger events. As shown in Figure 4, flurazepam had no significant effect on the rise time of either the small or large events (462 $\mu$s versus 395 $\mu$s and 461 $\mu$s versus 482 $\mu$s, respectively) but prolonged the decay time course of mIPSCs in both amplitude classes with, in this case, a somewhat greater effect on the decay of small mIPSCs. In five cells, the mean 62% decay time was increased from 9.0 $\pm$ 3.2 ms to 24.6 $\pm$ 10.9 ms for small mIPSCs ($<$140 pA; 166% $\pm$ 66% increase) and from 7.3 $\pm$ 0.9 ms to 16.0 $\pm$ 2.5 ms for large mIPSCs ($>$140 pA; 123% $\pm$ 55% increase). Although there was a tendency for small mIPSCs to decay more slowly than large ones, their decay was also more variable, and overall, the mean decay times and the percentage increases in flurazepam were not significantly different for the two classes of mIPSCs ($p > 0.05$, Student's t test). These results demonstrate that receptors underlying both small and large mIPSCs are benzodiazepine-sensitive, as would be predicted given the presence of $\alpha$1, $\beta$2, and $\gamma$2 subunits at each synapse. Nevertheless, as shown by the cumulative distributions in Figure 4D, the amplitude of the small mIPSCs was not changed by flurazepam, whereas that of the large mIPCS was significantly increased. Thus, postsynaptic $GABA_A$ receptors may not be fully occupied following the release of a packet of GABA at synapses generating "large" mIPSCs. An alternative possibility, that receptors at each site are saturated and that flurazepam, by increasing affinity of receptors for GABA, enables receptors at some sites to sense GABA released from neighboring synapses, is unlikely. First, this is not consistent with the differential effect of flurazepam on mIPSC amplitude and the lack of effect of flurazepam on mIPSC rise time. Secondly, overspill of GABA is unlikely to occur given the relatively low frequency of GABAergic synapses in these cells.

### Synaptic Channel Conductance

To determine how many channels underlie mIPSCs of different amplitudes, we analyzed fluctuations in their decay. Peak-scaled nonstationary fluctuation analysis (Figure 5A; Traynelis et al., 1993; De Koninck and Mody, 1994) was used to isolate fluctuations arising from stochastic channel closure from other sources of variance, such as differences in the number of channels exposed to the transmitter at different sites or variation in channel open probability from trial to trial. In five cells, we examined the relationship between mean current and peak-scaled variance. This was approximately parabolic (Figure 5B), and the initial slope of the relationship yielded an estimate for the weighted mean single-channel current of 2.16 $\pm$ 0.29 pA, corresponding to a weighted mean single-channel conductance for synaptic $GABA_A$ receptors of 27.1 $\pm$ 3.5 pS. This is similar to the single-channel conductance measured previously for extrasynaptic $GABA_A$ receptor channels in outside-out patches from stellate cells (28 pS; Llano and Gerschenfeld, 1993), consistent with the idea of receptor homogeneity. These data indicate that, in control conditions, individual mIPSCs can result from the opening of as few as six channels or as many as 380 channels. Moreover, this value for synaptic channel conductance, together with estimates of maximum channel open probability (see Discussion), and the differential effect of flurazepam allow us to suggest that a quantum of GABA saturates postsynaptic receptors at small synapses containing $<\sim$80 receptors but results in incomplete occupancy

and were contained within a complete series of 31 consecutive sections. Note the immunonegative asymmetrical synapse on the dendritic shaft indicated by an open arrow (in $A_2$).

(B) Serial sections ($B_1$–$B_9$) of a symmetrical synapse between an axon terminal (b) and an interneuron dendrite (d) showing an enrichment of immunoparticles within the synaptic specialization. An asymmetrical synapse (open arrows in $B_6$ and $B_7$) made by a bouton ($b_1$) with the same dendrite is immunonegative for the $GABA_A$ receptor subunit. The immunopositive symmetrical synapse was present in thirteen 60 nm thick sections. Note the consistency of the labeling throughout the sections and that the particles often appear clustered. Scale bar in (A) and (B), 0.2 $\mu$m.

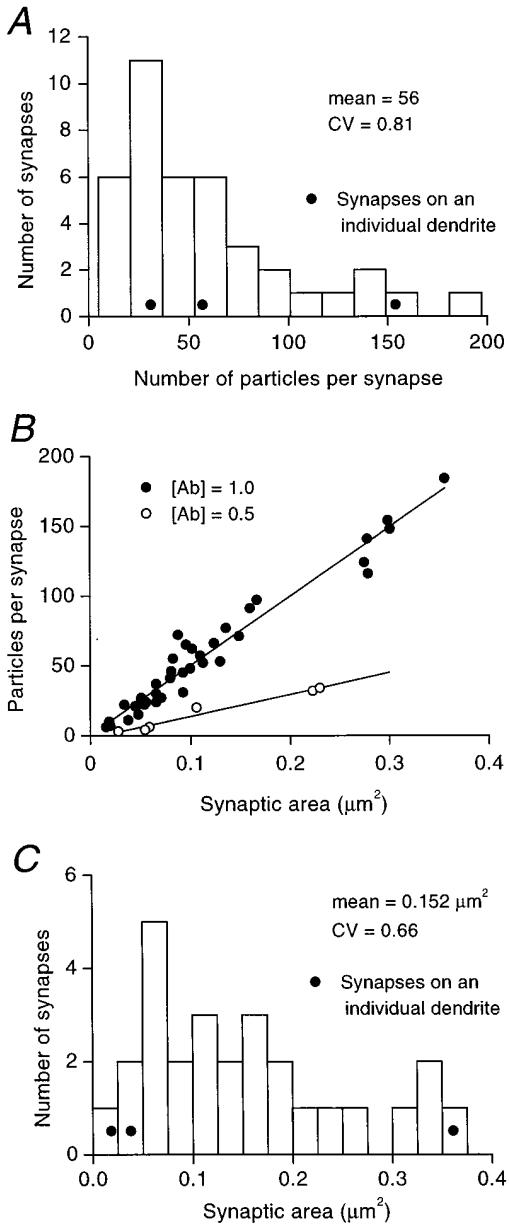


Figure 3. Large Variability in Synaptic Receptor Number and Uniform Receptor Density

(A) Distribution of symmetrical synapses on interneuron dendrites and somata according to their immunoreactivity for the $\alpha$1 subunit of the $GABA_A$ receptor. The distribution is skewed toward larger values with a 30-fold difference between the smallest (6) and the largest (184) number of immunoparticles per synapse (mean = 55.8 $\pm$ 44.9; CV = 0.81; n = 40). The closed circles denote immunoparticle numbers at three synapses converging onto a single dendrite (see Figure 2A) and demonstrate that the large variability in postsynaptic immunolabel is present in individual cells.

(B) Plot of immunoparticle number per synapse versus synaptic area for two different concentrations of primary antibody ([Ab] = 1.0, 6.3 $\mu$g protein/ml, n = 40; [Ab] = 0.5, 3.15 $\mu$g protein/ml, n = 6). In both cases, there is a positive linear relationship between imunoparticle number and synaptic area, with slopes of 495.8 and 157.0 particles/$\mu m^2$, respectively (Spearman rank-order correlation coefficients = 0.97 and 1). This linear correlation indicates a uniform receptor density across different synapses. Note that both regression lines intercept the ordinate close to zero (0.5 and $-1.8$).

(C) Histogram of areas of symmetrical synapses formed between GABA immunopositive axon terminals and GABA immunopositive interneuron dendrites in the molecular layer (osmium-treated, epoxy resin-embedded tissue). The distribution is skewed toward larger values (mean = 0.152 $\pm$ 0.01 $\mu m^2$; CV = 0.66; n = 27). The areas of three synapses converging onto an individual dendrite are indicated by closed circles.

at larger synapses containing a greater number of receptors.

### Relationship between mIPSC Amplitude and Synaptic Receptor Number

To determine whether the variation in receptor number at different synapses indicated by the immunolabeling could account for the spread of mIPSC amplitudes, we compared the distribution of gold particle number with the distribution of mIPSCs according to the number of channels open at their peak. As the former was derived from measurements of synapses on several postsynaptic neurons, we initially compared this with electrophysiological data pooled from all 12 recorded cells (Figures 6A and 6B). Both distributions exhibited similarly large variability (CV = 0.81 and 0.73), were significantly different from a Gaussian ($p < 0.05$, Shapiro-Wilk test), and were skewed toward larger values. For a more direct comparison of the shapes of distributions of gold particle and channel number, we used electrophysiological data from recordings made in the presence of flurazepam (n = 5), as our results suggested a greater degree of receptor occupancy in this condition. As shown in Figure 6C, when these data were standardized to a mean of zero and an SD of 1 (following the approach of Frerking et al., 1995), their distributions were not significantly different ($p > 0.05$, Kolmogorov-Smirnov test). Furthermore, synaptic area, which can be used as a measure of relative receptor content (Figure 3B), also had a distribution of similar shape (Figure 6C). Overall, these data suggest that variation in postsynaptic receptor number is the major determinant of mIPSC amplitude variability. The amplitude distribution of miniature postsynaptic currents recorded at the soma reflects not only the range of quantal amplitudes at different sites but also the frequency of vesicle release at each site (see Walmsley, 1995). Our data therefore also suggest that, in stellate cells at least, there is no correlation between the probability of release and quantal amplitude at different sites.

## Discussion

### Variability in Postsynaptic Responses Is a Consequence of the Variation in the Number of Receptors

Miniature IPSCs recorded from many central neurons vary remarkably in their peak amplitudes, generating skewed amplitude distributions (Edwards et al., 1990; Llano et al., 1991; Otis and Mody, 1992; Llano and Gerschenfeld, 1993; De Koninck and Mody, 1994; Pitler and Alger, 1994; Borst et al., 1994; Frerking et al., 1995; Soltesz et al., 1995; Hestrin and Armstrong, 1996; Poncer et al., 1996). This large variability is present in electrotonically compact cells (e.g., Borst et al., 1994), excluding the possibility that dendritic filtering alone accounts

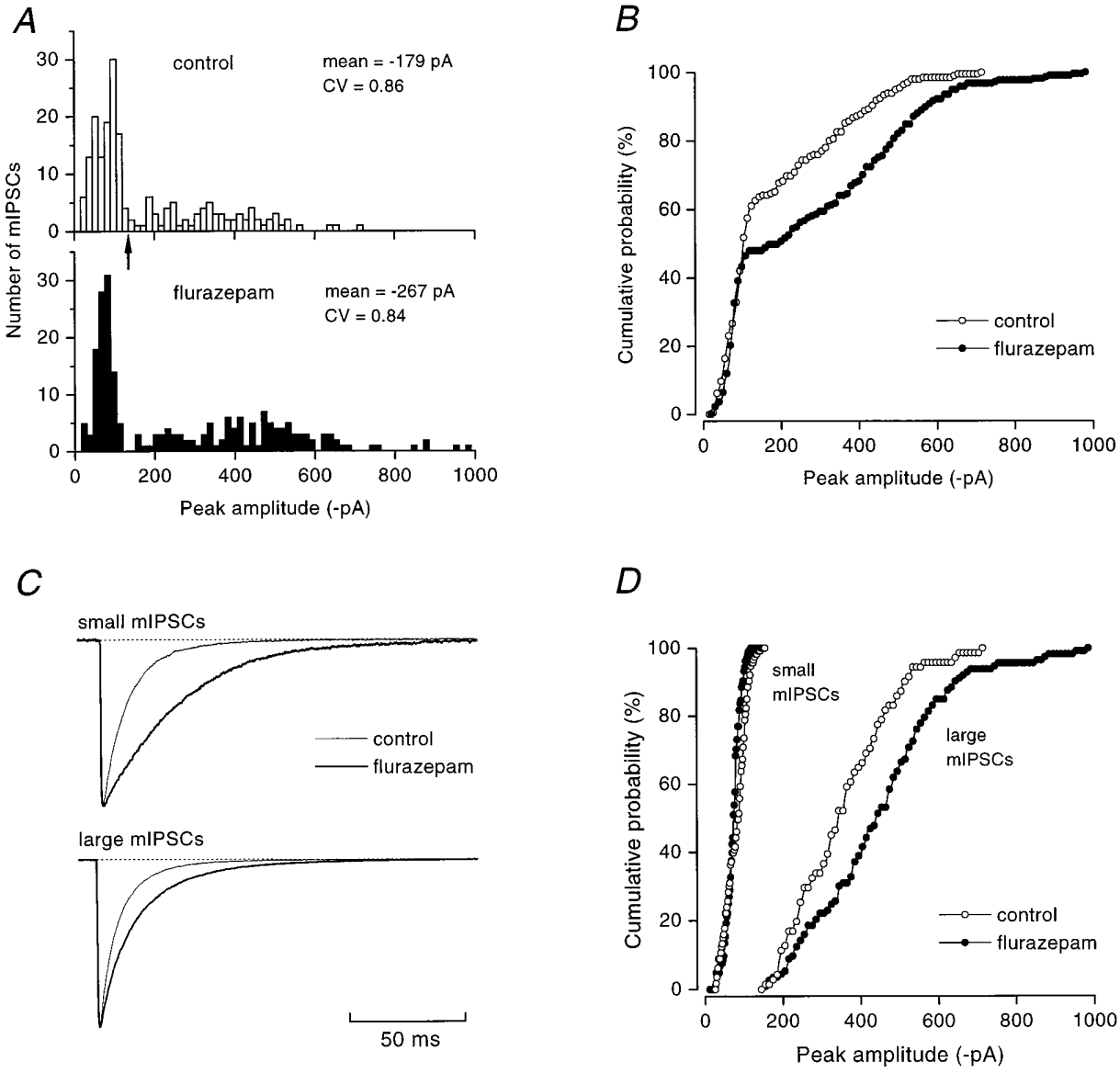


Figure 4. The Effects of Flurazepam on mIPSC Time Course and Amplitude

(A) Amplitude histograms of mIPSC recorded in control and flurazepam show that flurazepam (3 μM) significantly increased mean mIPSC amplitude ($p < 0.01$, Mann-Whitney U test), preferentially affecting the larger currents. The position of the first peak did not change after application of flurazepam, but the distribution of larger events was shifted to the right. P25 cell; recording conditions the same as in Figure 1.

(B) Cumulative probability plot of the amplitude of mIPSCs (the same as in [A]). The two distributions overlap up to ~140 pA but deviate from each other at larger amplitudes.

(C) Normalized average waveforms of "small" and "large" mIPSCs before and after application of flurazepam show that flurazepam prolonged the decay of mIPSCs in both amplitude classes. Events were arbitrarily divided into those smaller and greater than −140 pA in amplitude (arrow in upper panel of [A]). Control averages were generated from 116 and 71 events; flurazepam averages were from 104 and 81 events (small and large, respectively). For the averaged currents, the 62% decay time was increased from 11.0 to 34.3 ms for small mIPSCs and 8.1 to 15.0 ms for large mIPSCs.

(D) Cumulative probability plot of the amplitude of small and large mIPSCs (the same as in [C]). Although the decay time course of mIPSCs in both amplitude classes was prolonged, only the amplitude of the large mIPSC changed significantly after flurazepam application (from −353.6 ± 125.5 pA to −445.7 ± 172.1 pA; $p < 0.01$, Mann-Whitney U test). The amplitude of small mIPSCs remained unchanged (control −78.7 ± 29.3 pA; flurazepam -72.6 ± 20.2; $p > 0.05$).

for the variation in mIPSC amplitude (see also Soltesz et al., 1995). Multiquantal transmitter release (Ropert et al., 1990), variation in transmitter concentration (Frerking et al., 1995), stochastic channel gating (Faber et al., 1992), or differences in postsynaptic receptor number (Edwards et al., 1990; De Koninck and Mody, 1994; Borst et al., 1994) have been proposed as underlying causes of this quantal variability in different preparations. In the present study, we have investigated the origin of the unusually large variability in the amplitude of mIPSCs

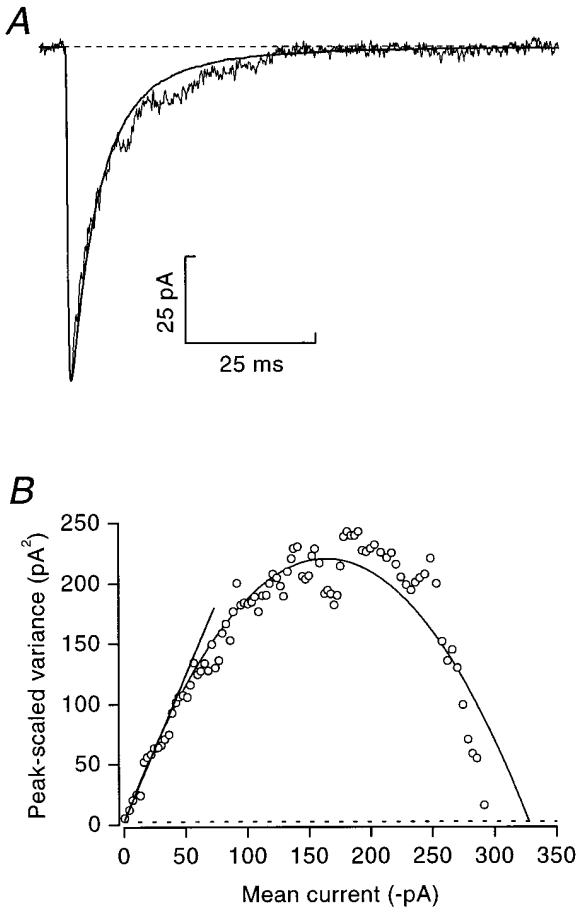


Figure 5. Determination of Synaptic Channel Conductance

(A) An individual mIPSC with the corresponding mean waveform (average of 65 events, smooth trace) superimposed and scaled to the same peak amplitude. Note the fluctuation of the individual mIPSC about the mean waveform, from which mean current and peak-scaled variance were calculated. Records of 250 ms duration were used for analysis, but for clarity only the first 100 ms of the current is shown.

(B) For the cell in (A), the initial slope of the relationship between mean current and peak-scaled variance (straight line) provided an estimate for the weighted mean single-channel current of 2.43 pA, corresponding to a channel conductance of 30 pS. This is similar to the estimate derived from the parabolic fit of the complete relationship (33 pS). The dotted line indicates the baseline current variance.

in cerebellar stellate cells, first described by Llano and Gerschenfeld (1993). This variability is particularly remarkable because one potential yet often neglected source of variance, different $GABA_A$ receptor subtypes at distinct synapses (Pearce, 1993; Koulen et al., 1996; Nusser et al., 1996), is unlikely. Stellate cells express only single $\alpha$, $\beta$, and $\gamma$ subunit types ($\alpha$1, $\beta$2 and $\gamma$2; Persohn et al., 1992; Somogyi et al., 1996), and in recombinant expression systems these three subunits preferentially coassemble into a single, benzodiazepine-sensitive receptor type (Pritchett et al., 1989; Angelotti and Macdonald, 1993; Tretter et al., 1997). Although such preferential coassembly is an important assumption for the interpretation of some of our results, the predicted receptor homogeneity that would result from such assembly is supported by several observations. Both small and large synapses contained all three subunit proteins (see Results and Somogyi et al., 1996), all mIPSCs were influenced by flurazepam, and synaptic (see Results) and extrasynaptic (Llano and Gerschenfeld, 1993) channels had a similar conductance of ~28 pS, as expected for receptors containing $\alpha$, $\beta$, and $\gamma$ subunits but not $\alpha$ and $\beta$ alone (e.g., main conductance states for $\alpha1\beta1\gamma2$S, 29 pS; $\alpha1\beta1$, 15 pS; Angelotti and Macdonald, 1993).

Overall, our immunocytochemical data indicate that in stellate cells postsynaptic $GABA_A$ receptors are present at a uniform density, and that there are synapses with widely differing areas and correspondingly different receptor content. Furthermore, we show that the variation in the postsynaptic receptor number parallels the variability in the amplitude of mIPSCs, with gold particle number, synaptic area, and mIPSC amplitude having similarly shaped, non-Gaussian distributions. Accordingly, we suggest that the major contribution to the variability in quantal amplitude is the variation in postsynaptic receptor number at different sites.

### Heterogeneity of Synapses According to Postsynaptic Receptor Occupancy

At the neuromuscular junction, although thousands of nicotinic receptors are activated by the quantal release of acetylcholine, these represent only a fraction of the available postsynaptic receptors (Katz and Miledi, 1972). Similarly, >1000 receptors are present opposite a release site at goldfish Mauthner cell synapses, yet not all of these become occupied upon the release of a quantum of glycine (Korn et al., 1987). By contrast, Edwards et al. (1990) suggested that the opening of only a small number (<30) of $GABA_A$ receptors underlies quantal events in hippocampal granule cells. In addition, because of the small quantal variance observed, these authors proposed that the synaptic $GABA_A$ receptors were saturated. Other studies have also shown that, on average, <60 $GABA_A$ receptors are present in the postsynaptic membranes at individual synapses of dentate granule cells (Otis and Mody, 1992; De Koninck and Mody, 1994), hippocampal hilar neurons (Soltesz and Mody, 1994), CA3 pyramidal cells (Poncer et al., 1996), and melanotropes from Xenopus laevis (Borst et al., 1994). Because benzodiazepine agonists failed to increase the peak amplitude of mIPSCs, several of these authors concluded that the release of a quantum of GABA results in complete occupancy of postsynaptic receptors (Otis and Mody, 1992; De Koninck and Mody, 1994; Soltesz and Mody, 1994; Poncer et al., 1996). However, using an identical pharmacological approach in cultured retinal amacrine cells, Frerking et al. (1995) observed an increase in mIPSC amplitude and suggested that transmitter does not saturate the estimated 10–30 $GABA_A$ receptors present at these synapses. On the basis of this and other evidence, these authors concluded that variability in mIPSC amplitude was a consequence of variation in transmitter concentration.

Our results in cerebellar stellate cells suggest that these different forms of synaptic operation can be observed at different synapses on a single cell. This conclusion is based on the observation that a benzodiazepine agonist, flurazepam, differentially affected the peak

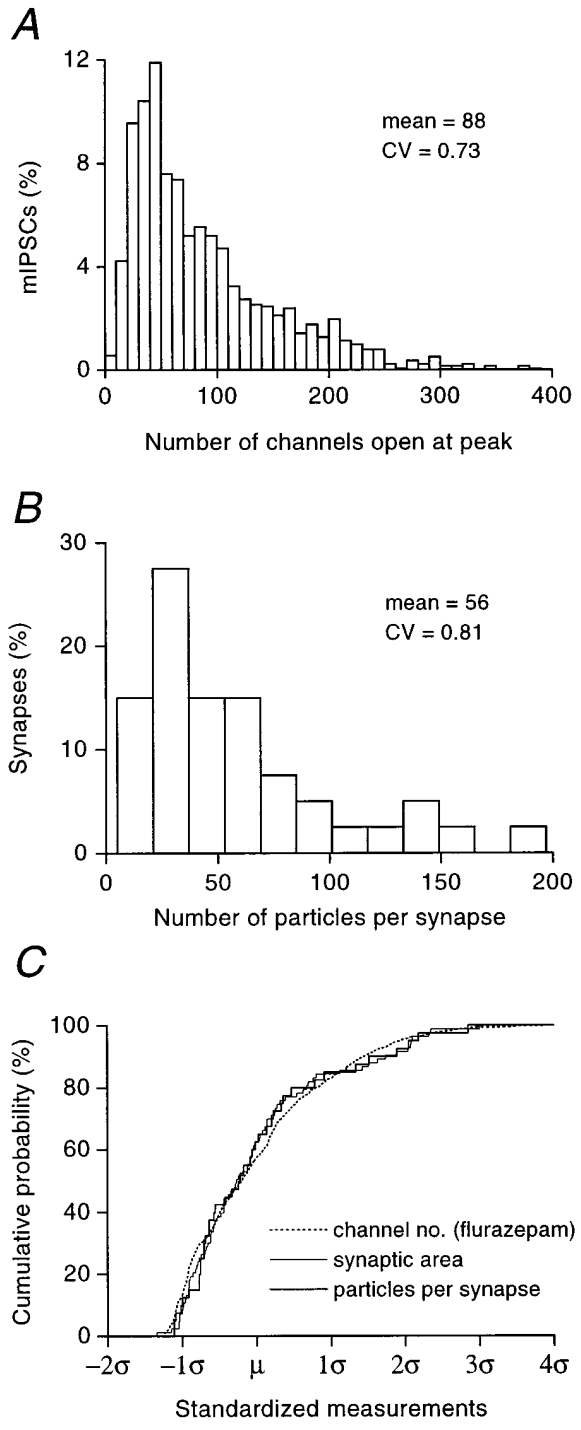


Figure 6. Comparison of Synaptic Channel Number and Immunoreactive Receptor Number

(A and B) Comparison of the distribution of mIPSCs according to the number of channels open at their peak (pooled data from all 12 cells; n = 1422) with the distribution of synapses according to their immunoreactive $\alpha$1 subunit content (n = 40; data from Figure 3A). The number of channels open at the peak was derived by dividing mIPSC peak amplitude by the estimated synaptic single-channel current (*i*). Neither distribution is Gaussian but both are skewed toward larger values and display similarly large coefficients of variation.

(C) Standardized cumulative probability distributions (mean, $\mu$ = 0; SD, $\sigma$ = 1) of the number of channels open at the peak of the mIPSCs recorded in the presence of flurazepam ("channel no."; pooled data from five cells; n = 947), immunoparticles per synapse, and synaptic area. Synaptic areas were measured from epoxy and Lowicryl resin-embedded tissue and pooled after standardization (n = 27 and 56 synapses, respectively). The shapes of the distributions are not significantly different from one another ($p > 0.05$, Kolmogorov-Smirnov test), suggesting that variation in the number of receptors at different synapses underlies the variability in mIPSC amplitude.

amplitude of "small" and "large" mIPSCs; currents of $>\sim$140 pA were increased in amplitude, while smaller ones were not. The existence of two populations of mIPSCs, differentially affected by flurazepam yet originating from a common receptor type, makes it unlikely that the observed increase in mIPSC amplitude could result from an increase in the maximum open probability of the underlying channels ($P_{o,max}$; as defined by Silver et al., 1996). Rather, the most parsimonious explanation for these results is that the receptors giving rise to the two populations of mIPSCs differ in the degree to which they are occupied following the release of single quanta, and that this difference is determined by the size of the synapse and the number of postsynaptic receptors present. We estimate that the critical number of synaptic receptors below which all of the receptors are occupied is $\sim$80 (corresponding, in stellate cells, to a synaptic area of $\sim$0.06 $\mu m^2$; see below). This number is derived from the amplitude criterion used to distinguish different populations of mIPSCs (140 pA), our measurement of synaptic channel current (2.16 pA), and published values of $GABA_A$ receptor $P_{o,max}$ ($\sim$0.8; Newland et al., 1991; Jones and Westbrook, 1995). This finding is consistent with the idea that the generally low numbers of postsynaptic $GABA_A$ receptors present at central synapses (30–60) are saturated following synaptic release of GABA (Edwards et al., 1990; Otis and Mody, 1992; De Koninck and Mody, 1994; Soltesz and Mody, 1994; Poncer et al., 1996).

In stellate cells, the majority of mIPSCs ($\sim$55%) have a peak amplitude of >140 pA and must arise at synapses containing >80 receptors. The large number of receptors at such sites and the correspondingly large cleft volume could combine to allow the generation of large mIPSCs in the absence of receptor saturation. For example, if a saturating concentration of GABA arose following the rapid equilibration of GABA within the smallest synaptic volumes we observed, then at the largest synapses the corresponding concentration would be 20- to 25-fold less. Clearly, this is a highly simplified view; and, as pointed out by Frerking and Wilson (1996b), it is difficult to say much about the degree of receptor occupancy on the basis of peak transmitter concentration without knowing the time course of transmitter clearance. Nevertheless, as the transmitter transient is likely to be very brief (e.g., Clements, 1996), even the relatively high steady-state affinity of neuronal $GABA_A$ receptors ($EC_{50}$, $\sim$20 $\mu$M) need not be incompatible with a lack of saturation at the larger synapses. Parenthetically, the similarly rapid rise time of small and large mIPSCs in stellate cells does not counter this argument; a rapid rise time would only imply a high concentration of transmitter in the cleft if transmitter were present long enough

to equilibrate with the receptors (Frerking and Wilson, 1996b). Differences in the transmitter content of different vesicles, as well as possible variations in the precise location of vesicle release within the synaptic junction, are likely to result in some additional variability in the amplitude of mIPSCs arising at these large synapses.

### The Density of Synaptic $GABA_A$ Receptors Is Uniform in Stellate Cells

A particularly intriguing observation to emerge from the present study is that the density of $GABA_A$ receptors is uniform across all synapses. This is indicated by the positive, linear correlation between the number of immunoreactive $GABA_A$ receptor subunits and the area of synaptic specializations. Little is known about how such a uniform receptor density might be achieved. For nicotinic acetylcholine, glycine, and glutamate receptors, it has been suggested that intracellular, receptor-associated proteins (e.g., 43K protein, gephyrin, PSD-95, GRIP, and Homer) are needed for their clustering at the synapse (reviewed by Froehner, 1993; Kirsch et al., 1996; Sheng, 1997). Although no such $GABA_A$ receptor-associated protein has been conclusively identified, gephyrin-like immunoreactivity has been shown at GABAergic synapses (Sassoe-Pognetto et al., 1995), suggesting that either gephyrin or a gephyrin-like protein may play a similar role for $GABA_A$ receptors. Such proteins could provide a highly organized subsynaptic matrix to which only a defined number of $GABA_A$ receptors would be coupled. The precise organization of receptors within the synaptic junction could also be subject to regulation (Nusser et al., 1994). For example, although receptor density appears uniform when calculated across all synaptic specializations, this does not preclude an uneven distribution within individual specializations. Indeed, in most stellate cell synapses, immunoparticles were not evenly distributed within a given junctional membrane but often formed what appeared to be "microclusters".

In stellate cells, the mean number of channels open at the peak of mIPSCs recorded in flurazepam is calculated to be 113, which, assuming a $P_{o,max}$ of 0.8, corresponds to the presence of ~140 postsynaptic receptors. As the mean number of immunoparticles per synapse is 56, one immunoparticle represents ~2.5 synaptic $GABA_A$ receptors. This is likely to be a slight underestimate because, as seen from the physiological results, the postsynaptic receptors at sites of origin of large mIPSCs may not be saturated, even in the presence of flurazepam. The relatively high immunolabeling efficiency may result from the fact that each $GABA_A$ receptor contains two $\alpha$ subunits (Chang et al., 1996; Tretter et al., 1997); thus, one particle would correspond to approximately five synaptic $\alpha$1 subunits. This ratio, of course, depends on the primary and secondary antibodies and on other technical factors, such as the fixation condition and the type of resin employed. Nevertheless, the density of synaptic $GABA_A$ receptors can be calculated by multiplying the immunoparticle density (496 particles per $\mu m^2$) by 2.5, resulting in an estimated 1250 receptors per $\mu m^2$. This value is much lower than that obtained for nicotinic acetylcholine receptors at the neuromuscular junction (8,000–10,000 receptors per $\mu m^2$; Fertuck and Salpeter, 1974), suggesting that $GABA_A$ receptor packing density is not maximal. It will be of interest to determine whether the density of synaptic $GABA_A$ receptors is similar for all cell types and whether a uniform receptor density across different synapses is a general rule for other ionotropic amino acid neurotransmitter receptors.

## Experimental Procedures

### Tissue Preparation for Electrophysiology

Sagittal slices of the cerebellar vermis were prepared from P13–P26 Sprague-Dawley rats as previously described (Kaneda et al., 1995). Briefly, rats were decapitated, and the brains were removed and placed into ice-cold slicing solution, which contained (in mM): 25 NaCl, 2.5 KCl, 1 $CaCl_2$, 4 $MgCl_2$, 1.25 $NaH_2PO_4$, 26 $NaHCO_3$, 25 glucose, and 4 lactate (pH 7.4 when bubbled with 95% $O_2$–5% $CO_2$). Slices (250–350 $\mu$m thick) were cut with a vibrating microslicer (DTK-1000, Dosaka EM Company Limited, Kyoto, Japan) and were incubated at 30°C for 1 hr prior to recording.

During recording, slices were continuously perfused with a solution containing (in mM): 125 NaCl, 2.5 KCl, 2 $CaCl_2$, 1 $MgCl_2$, 1.25 $NaH_2PO_4$, 26 $NaHCO_3$, 25 glucose, and 4 lactate (pH 7.4 when bubbled with 95% $O_2$–5% $CO_2$). The pipette solution contained (in mM): 140 CsCl, 4 NaCl, 0.5 $CaCl_2$, 2 Mg-ATP, 10 HEPES, and 5 EGTA (adjusted to pH 7.3 with CsOH). In all experiments, 10 $\mu$M D-2-amino-5-phosphonopentanoic acid (D-AP5; Tocris Cookson, Bristol, UK), 5 $\mu$M 6-cyano-7-nitroquinoxaline-2,3-dione (CNQX; Tocris Cookson), and 300 nM strychnine (Sigma, Poole, UK) were added to the perfusion medium to prevent the activation of N-methyl-D-aspartate (NMDA) and non-NMDA type glutamate receptors and glycine receptors, respectively. Other drugs used were 10 $\mu$M bicuculline methobromide (Tocris Cookson), 0.5 $\mu$M tetrodotoxin (TTX; Sigma), and 3 $\mu$M flurazepam (Sigma).

Whole-cell patch-clamp recordings were made at room temperature from the soma of visually identified neurons located in the outer two-thirds of the molecular layer (Zeiss Axioscop FS differential interference optics, 40× water immersion objective). Recordings were obtained with an Axopatch 200A patch-clamp amplifier (Axon Instruments, Foster City, CA). Patch pipettes were made from thick-walled borosilicate glass (GC-150F; Clark Electromedical, Pangbourne, UK), coated with Sylgard resin (Dow Corning 184), and fire polished to a resistance of 6–12 M$\Omega$ when filled with pipette solution. Cells were accepted as stellate cells only if large currents (due to the spontaneous firing of action potentials) were observed during seal formation and if spontaneous synaptic currents were present after establishing the whole-cell recording (Llano and Gerschenfeld, 1993). The 12 cells (P18–P26) analyzed in detail had an input resistance of 1.65 ± 2.22 G$\Omega$ and a whole-cell capacitance of 4.5 ± 1.4 pF. The series resistance remaining after 60%–75% compensation was 8.0 ± 2.3 M$\Omega$.

### Data Analysis

Spontaneously occurring IPSCs were recorded on digital audio tape (BioLogic DTR-1204, DC to 20 kHz). For analysis, currents were filtered at 2 kHz (−3 db, 8-pole Bessel filter) and digitized at 10 kHz (Axotape, pCLAMP 6.1, Axon Instruments). mIPSCs were identified by eye from the digitized records and were analyzed using software (N v1.0) written by Stephen Traynelis (Emory University, Atlanta). For some cells, records were reanalyzed using a threshold-based event detection algorithm (WCP v1.2; courtesy of John Dempster, Strathclyde University, Glasgow, UK). The two methods gave similar results. For each cell, average mIPSC waveforms were generated from >50 events aligned on the point of steepest rise. Current decays were fitted using either N or Origin 4.10 (Microcal, Northampton, MA). Results are given as mean ± SD.

To determine the conductance of synaptic $GABA_A$ channels, mIPSCs were analyzed by nonstationary fluctuation analysis. To isolate fluctuations in the current decay due to stochastic channel gating, the mean waveform was scaled to the peak of individual mIPSCs (Traynelis et al., 1993; Silver et al., 1996). The requirements for such analysis include the stability of current decay time course

throughout the recording and the absence of any correlation between decay time course and peak amplitude. The relationship between the peak-scaled variance and the mean current is given by

$$\sigma^2_{PS} = i\bar{I} - \bar{I}^2/N_P + \sigma^2_B,$$

where $\sigma^2_{PS}$ is the peak-scaled variance, $\bar{I}$ is the mean current, $i$ is the weighted mean single-channel current, $N_P$ is the number of channels open at the peak of the IPSC, and $\sigma^2_B$ is the background variance. In these experiments, 31–69 mIPSCs were analyzed from selected epochs in each of five cells in which there was no correlation between current decay (62% decay time) and peak amplitude ($p > 0.05$, Spearman rank-order correlation test). The weighted mean single-channel current can be estimated by fitting the full parabola or the initial slope of the relationship, if this is skewed (Traynelis et al., 1993). In those cases where the $\sigma^2_{PS} - \bar{I}$ relationships were not skewed, estimates of the single-channel current were similar for both methods (see Figure 5B). However, because some of the $\sigma^2_{PS} - \bar{I}$ relationships were skewed, in all cases, the initial part of the plot was fitted to give $i$, while $N_P$ was calculated from $\bar{I}/i$.

### Tissue Preparation for Immunocytochemistry

Five adult Wistar rats (~150 g) were anesthetized with Sagatal (pentobarbitone sodium, 220 mg/kg intraperitoneally) and perfused through the heart with saline, followed by fixative containing 4% paraformaldehyde, 0.05%–0.2% glutaraldehyde, and ~0.2% picric acid for 13–25 min. After perfusion, the brains were removed, and blocks from the cerebella were cut out and either postfixed in the same fixative for 2 hr or washed in several changes of 0.1 M phosphate buffer (PB). Freeze substitution and low temperature embedding in Lowicryl resin was carried out as described earlier (Baude et al., 1993; Nusser et al., 1995b). Briefly, 500 μm thick Vibratome sections were cut and washed in PB overnight. The sections were placed into 1 M sucrose solution in PB for 2 hr for cryoprotection before they were slammed into a copper block cooled in liquid $N_2$. This was followed by freeze-substitution with methanol and embedding in Lowicryl HM 20 (Chemische Werke Lowi GMBH, Germany). Two further rats were anesthetized with Sagatal and transcardially perfused with saline, followed by a fixative containing 2% paraformaldehyde and 2.5% glutaraldehyde in PB. After perfusion, the brains were removed and washed in PB, and 60–100 μm sagittal sections were cut from the vermis of the cerebellum with a Vibratome and processed for electron microscopy (Nusser et al., 1995b). The sections were postfixed in 1% osmium tetroxide (dissolved in PB) for 40 min and contrasted with uranyl acetate (dissolved in water), followed by dehydration and flat-embedding in Durcupan ACM (Fluka) resin.

### Antibodies and Controls

Rabbit polyclonal antibody (code number P16) was raised to a synthetic peptide corresponding to residues 1–9 of the rat α1 subunit. Antibody specificity has been described earlier (Zezula et al., 1991). Immunoreactions on Lowicryl resin-embedded ultrathin sections with affinity-purified P16 antibody were carried out at a final protein concentration of 3.15 or 6.3 μg/ml. Mouse monoclonal antibody (code number bd17; Haring et al., 1985) recognising the β2 and β3 subunits of the $GABA_A$ receptors was used at a protein concentration of 10 or 20 μg/ml (Boehringer Mannheim GmBH, Mannheim, Germany). Rabbit antiserum to GABA (code number 9; see Hodgson et al., 1985 for antibody specificity) was used at dilutions of 1:2000 and 1:3000 on epoxy resin-embedded ultrathin sections. Selective labeling, resembling that obtained with the specific antibodies, could not be detected when the primary antibodies were either omitted or replaced by 5% normal rabbit serum.

### Postembedding Immunocytochemistry for $GABA_A$ Receptor Subunits

Postembedding immunocytochemistry was carried out on 60 nm thick sections of slam-frozen, freeze-substituted, Lowicryl-embedded cerebella from five rats (Nusser et al., 1995b). The sections were picked up on pioloform-coated nickel grids and incubated on drops of blocking solution (Tris-buffered saline [TBS]; pH = 7.4; containing 20% normal goat serum) for 30 min, followed by incubation on drops of primary antibodies (diluted in TBS containing 5% normal goat serum and 0.1% cold water fish skin gelatin) overnight. The sections were then washed and incubated on drops of goat anti-rabbit IgG coupled to 1.4 nm gold particles (diluted 1:100; Nanoprobes Incorporated, Stony Brook, NY) for 2 hr at room temperature. Following several washes, sections were fixed in a 2% glutaraldehyde solution for 2 min and then transferred to drops of ultra pure water prior to silver enhancement in the dark with HQ Silver kit for 4–5 min. After further washing in ultra pure water, the sections were contrasted with saturated aqueous uranyl acetate, followed by staining with lead citrate.

### Quantification of Immunoreactivity for $GABA_A$ Receptor Subunits

Measurements were taken from a well preserved strip of Lowicryl-embedded ultrathin sections (tissue from one animal) immunoreacted for the α1 subunit of the $GABA_A$ receptor. The molecular layer was searched systematically until an interneuron dendrite was found. A dendrite was classified as belonging to an interneuron if it received several asymmetrical synapses on its shaft, rarely emitted spines, and contained no cisternal stacks. Every symmetrical synaptic junction on these dendrites was photographed and followed on serial ultrathin sections completely through the synaptic specialization. Immunoparticles were counted within the anatomically defined synaptic junctions (Gray, 1959). The length of the junction was also measured on each ultrathin section. The synaptic area was calculated by multiplying the synaptic length in each section with the thickness of the electron microscopic section (e.g., 60 nm); areas were then summed for all sections through which each synapse was present. The synaptic area and number of particles per synapse were correlated by the Spearman rank-order test, and immunoparticle density (particles per $\mu m^2$) was determined by standard linear regression.

### Postembedding Immunocytochemistry for GABA and Measurement of Synaptic Areas

Measurements were taken from osmium-treated, epoxy resin-embedded cerebella of two rats. Ten to fifteen serial ultrathin sections (65 nm thick) were cut and picked up on a pioloform-coated copper grid. The next section was picked up on a nickel grid and the following 10–15 sections on a copper grid again. Sections on nickel grids were immunoreacted for GABA as described earlier (Somogyi and Hodgson, 1985). After treatment with 1% periodic acid (dissolved in water) for 8 min, followed by washing and treatment with 2% sodium periodate (dissolved in water) for 10 min, the grids were then transferred onto drops of blocking solution for 2 hr and then incubated in a solution of polyclonal antibody to GABA (diluted in TBS containing 1% normal goat serum) for 2 hr, followed by washing and incubation on drops of goat anti-rabbit IgG coupled to 15 nm gold particles (BioClin Services Limited, Cardiff, UK). After further washing in water, the sections were contrasted with saturated aqueous uranyl acetate, followed by staining with lead citrate. Treated sections were systematically searched until a GABA immunopositive interneuron dendrite (for criteria see above) was found in the molecular layer. Symmetrical synapses between this dendrite and GABA immunopositive axon terminals were photographed and followed on serial sections until they disappeared. The length of the synaptic junction was measured on each ultrathin section and the synaptic area was calculated by multiplying each length with the thickness of the section.

### Acknowledgments

This work was supported by the Medical Research Council, the Wellcome Trust, the Howard Hughes Medical Institute (International Scholars Award to S. C.-C.), and a European Commission Shared Cost RTD Programme Grant (number $BIO_4CT96$–0585). We are grateful to Werner Sieghart and Peter Somogyi for providing antibody P16 and antiserum GABA number 9, respectively. We would like to thank Brian Edmonds, Matthew Frerking, Michael Häusser, David Rossi, Angus Silver, and Peter Somogyi for valuable discussions and David Attwell, Stephen Brickley, Akiko Momiyama, Angus Silver, and Peter Somogyi for comments on the manuscript. We would also like to thank Stephen Traynelis and Ioana Vais for provision of

software and Zahida Ahmad, Juliann Thomas, Paul Jays, and Frank Kennedy for technical assistance.

Received June 4, 1997; revised August 1, 1997.

**References**

Angelotti, T.P., and Macdonald, R.L. (1993). Assembly of $GABA_A$ receptor subunits: $\alpha1\beta1$ and $\alpha1\beta1\gamma2s$ subunits produce unique ion channels with dissimilar single-channel properties. J. Neurosci. *13*, 1429–1440.

Baude, A., Nusser, Z., Roberts, J.D.B., Mulvihill, E., McIlhinney, R.A.J., and Somogyi, P. (1993). The metabotropic glutamate receptor (mGluR1$\alpha$) is concentrated at perisynaptic membrane of neuronal subpopulations as detected by immunogold reaction. Neuron *11*, 771–787.

Bekkers, J.M., and Stevens, C.F. (1995). Quantal analysis of EPSCs recorded from small numbers of synapses in hippocampal cultures. J. Neurophysiol. *73*, 1145–1156.

Bekkers, J.M., Richerson, G.B., and Stevens, C.F. (1990). Origin of variability in quantal size in cultured hippocampal neurons and hippocampal slices. Proc. Natl. Acad. Sci. USA *87*, 5359–5362.

Bier, M., Kits, K.S., and Borst, J.G.G. (1996). Relation between rise times and amplitudes of GABAergic postsynaptic currents. J. Neurophysiol. *75*, 1008–1012.

Borst, J.G.G., Lodder, J.C., and Kits, K.S. (1994). Large amplitude variability of GABAergic IPSCs in melanotropes from Xenopus laevis: evidence that quantal size differs between synapses. J. Neurophysiol. *71*, 639–655.

Brickley, S.G., Cull-Candy, S.G., and Farrant, M. (1996). Development of a tonic form of synaptic inhibition in rat cerebellar granule cells resulting from persistent activation of $GABA_A$ receptors. J. Physiol. (Lond.) *497*, 753–759.

Chang, Y., Wang, R., Barot, S., and Weiss, D.S. (1996). Stoichiometry of a recombinant $GABA_A$ receptor. J. Neurosci. *16*, 5415–5424.

Clements, J.D. (1996). Transmitter timecourse in the synaptic cleft: its role in central synaptic function. Trends Neurosci. *19*, 163–171.

De Koninck, Y., and Mody, I. (1994). Noise analysis of miniature IPSCs in adult rat brain slices: properties and modulation of synaptic $GABA_A$ receptor channels. J. Neurophysiol. *71*, 1318–1335.

del Castillo, J., and Katz, B. (1954). Quantal components of the end-plate potential. J. Physiol. (Lond.) *124*, 560–573.

Edwards, F.A. (1995). Anatomy and electrophysiology of fast central synapses lead to a structural model for long-term potentiation. Physiol. Rev. *75*, 759–787.

Edwards, F.A., Konnerth, A., and Sakmann, B. (1990). Quantal analysis of inhibitory synaptic transmission in dentate gyrus of rat hippocampal slices: a patch-clamp study. J. Physiol. (Lond.) *430*, 213–249.

Faber, D.S., Young, W.S., Legendre, P., and Korn, H. (1992). Intrinsic quantal variability due to stochastic properties of receptor-transmitter interactions. Science *258*, 1494–1498.

Fertuck, H.C., and Salpeter, M.M. (1974). Localization of acetylcholine receptor by $^{125}$I-labeled $\alpha$ bungarotoxin binding at mouse motor endplates. Proc. Natl. Acad. Sci. USA *71*, 1376–1378.

Frerking, M., and Wilson, M. (1996a). Effects of variance in mini amplitude on stimulus-evoked release—a comparison of 2 models. Biophys. J. *70*, 2078–2091.

Frerking, M., and Wilson, M. (1996b). Saturation of postsynaptic receptors at central synapses? Curr. Opin. Neurobiol. *6*, 395–403.

Frerking, M., Borges, S., and Wilson, M. (1995). Variation in GABA mini amplitude is the consequence of variation in transmitter concentration. Neuron *15*, 885–895.

Froehner, S.C. (1993). Regulation of ion channel distribution at synapses. Annu. Rev. Neurosci. *16*, 347–368.

Gray, E.G. (1959). Axo-somatic and axo-dendritic synapses of the cerebral cortex: an electron microscope study. J. Anat. *93*, 420–433.

Gulyas, A.I., Miles, R., Sik, A., Toth, K., Tamamaki, N., and Freund, T.F. (1993). Hippocampal pyramidal cells excite inhibitory neurons through a single release site. Nature *366*, 683–687.

Haring, P., Stahli, C., Schoch, P., Takacs, B., Staehelin, T., and Mohler, H. (1985). Monoclonal antibodies reveal structural homogeneity of $\gamma$-aminobutyric acid/benzodiazepine receptors in different brain areas. Proc. Natl. Acad. Sci. USA *82* 4837–4841.

Hestrin, S., and Armstrong, W.E. (1996). Morphology and physiology of cortical neurons in layer I. J. Neurosci. *16*, 5290–5300.

Hodgson, A.J., Penke, B., Erdei, A., Chubb, I.W., and Somogyi, P. (1985). Antisera to $\gamma$-aminobutyric acid. I. Production and characterization using a new model system. J. Histochem. Cytochem. *33*, 229–239.

Jack, J.J.B., Larkman, A.U., Major, G., and Stratford, K.J. (1994). Quantal analysis of the synaptic excitation of CA1 hippocampal pyramidal cells. In Molecular and Cellular Mechanisms of Neurotransmitter Release, L. Stjarne, P. Greengard, S. Grillner, T. Hokfelt, and D. Ottoson, eds. (New York: Raven Press), pp. 275–299.

Jones, M.V., and Westbrook, G.L. (1995). Desensitized states prolong $GABA_A$ channel responses to brief agonist pulses. Neuron *15*, 181–191.

Kaneda, M., Farrant, M., and Cull-Candy, S.G. (1995). Whole-cell and single channel currents activated by GABA and glycine in granule cells of the rat cerebellum. J. Physiol. (Lond.) *485*, 419–435.

Katz, B., and Miledi, R. (1972). The statistical nature of the acetylcholine potential and its molecular components. J. Physiol. (Lond.) *224*, 665–699.

Kirsch, J., Meyer, G., and Betz, H. (1996). Synaptic targeting of ionotropic neurotransmitter receptors. Mol. Cell. Neurosci. *8*, 93–98.

Korn, H., Burnod, Y., and Faber, D.S. (1987). Spontaneous quantal currents in central neuron match predictions from binomial analysis of evoked responses. Proc. Natl. Acad. Sci. USA *84*, 5981–5985.

Koulen, P., Sassoe-Pognetto, M., Grunert, U., and Wassle, H. (1996). Selective clustering of $GABA_A$ and glycine receptors in the mammalian retina. J. Neurosci. *16*, 2127–2140.

Lavoie, A.M., and Twyman, R.E. (1996). Direct evidence for diazepam modulation of $GABA_A$ receptor microscopic affinity. Neuropharmacology *35*, 1383–1392.

Liu, G., and Tsien, R.W. (1995). Properties of synaptic transmission at single hippocampal synaptic boutons. Nature *375*, 404–408.

Llano, I., and Gerschenfeld, H.M. (1993). Inhibitory synaptic currents in stellate cells of rat cerebellar slices. J. Physiol. (Lond.) *468*, 177–200.

Llano, I., Leresche, N., and Marty, A. (1991). Calcium entry increases the sensitivity of cerebellar Purkinje cells to applied GABA and decreases inhibitory synaptic currents. Neuron *6*, 565–574.

Matsubara, A., Laake, J.H., Davanger, S., Usami, S., and Ottersen, O.P. (1996). Organization of AMPA receptor subunits at a glutamate synapse: a quantitative immunogold analysis of hair cell synapses in the rat organ of Corti. J. Neurosci. *16*, 4457–4467.

Newland, C.F., Colquhoun, D., and Cull-Candy, S.G. (1991). Single channels activated by high concentrations of GABA in superior cervical ganglion neurones of the rat. J. Physiol. (Lond.) *432*, 203–233.

Nusser, Z., Mulvihill, E., Streit, P., and Somogyi, P. (1994). Subsynaptic segregation of metabotropic and ionotropic glutamate receptors as revealed by immunogold localization. Neuroscience *61*, 421–427.

Nusser, Z., Roberts, J.D.B., Baude, A., Richards, J.G., and Somogyi, P. (1995a). Relative densities of synaptic and extrasynaptic $GABA_A$ receptors on cerebellar granule cells as determined by a quantitative immunogold method. J. Neurosci. *15*, 2948–2960.

Nusser, Z., Roberts, J.D.B., Baude, A., Richards, J.G., Sieghart, W., and Somogyi, P. (1995b). Immunocytochemical localization of the $\alpha1$ and $\beta2/3$ subunits of the $GABA_A$ receptor in relation to specific GABAergic synapses in the dentate gyrus. Eur. J. Neurosci. *7*, 630–646.

Nusser, Z., Sieghart, W., Benke, D., Fritschy, J.-M., and Somogyi, P. (1996). Differential synaptic localization of two major $\gamma$-aminobutyric acid type A receptor $\alpha$ subunits on hippocampal pyramidal cells. Proc. Natl. Acad. Sci. USA *93*, 11939–11944.

Otis, T.S., and Mody, I. (1992). Modulation of decay kinetics and

frequency of GABA-receptor-mediated spontaneous inhibitory postsynaptic currents in hippocampal neurons. Neuroscience *49*, 13–32.

Palay, S.L., and Chan-Palay, V. (1974). Cerebellar Cortex: Cytology and Organization (Berlin: Springer).

Pearce, R.A. (1993). Physiological evidence for two distinct $GABA_A$ responses in rat hippocampus. Neuron *10*, 189–200.

Persohn, E., Malherbe, P., and Richards, J.G. (1992). Comparative molecular neuroanatomy of cloned $GABA_A$ receptor subunits in the rat CNS. J. Comp. Neurol. *326*, 193–216.

Pierce, J.P., and Mendell, L.M. (1993). Quantitative ultrastructure of Ia boutons in the ventral horn: scaling and positional relationships. J. Neurosci. *13*, 4748–4763.

Pitler, T.A., and Alger, B.E. (1994). Depolarization-induced suppression of GABAergic inhibition in rat hippocampal pyramidal cells: G protein involvement in a presynaptic mechanism. Neuron *13*, 1447–1455.

Poncer, J.-C., Durr, R., Gahwiler, B.H., and Thompson, S.M. (1996). Modulation of synaptic $GABA_A$ receptor function by benzodiazepines in area CA3 of rat hippocampal slice cultures. Neuropharmacology *35*, 1169–1179.

Popratiloff, A., Weinberg, R.J., and Rustioni, A. (1996). AMPA receptor subunits underlying terminals of fine-caliber primary afferent fibers. J. Neurosci. *16*, 3363–3372.

Pritchett, D.B., Sontheimer, H., Shivers, B.D., Ymer, S., Kettenmann, H., Schofield, P.R., and Seeburg, P.H. (1989). Importance of a novel $GABA_A$ receptor subunit for benzodiazepine pharmacology. Nature *338*, 582–585.

Rogers, C.J., Twyman, R.E., and Macdonald, R.L. (1994). Benzodiazepine and $\beta$-carboline regulation of single $GABA_A$ receptor channels of mouse spinal neurones in culture. J. Physiol. (Lond.) *475*, 69–82.

Ropert, N., Miles, R., and Korn, H. (1990). Characteristics of miniature inhibitory postsynaptic currents in CA1 pyramidal neurones of rat hippocampus. J. Physiol. (Lond.) *428*, 707–722.

Sassoe-Pognetto, M., Kirsch, J., Grunert, U., Greferath, U., Fritschy, J.-M., Mohler, H., Betz, H., and Wassle, H. (1995). Colocalization of gephyrin and $GABA_A$-receptor subunits in the rat retina. J. Comp. Neurol. *356*, 1–14.

Sheng, M. (1997). Glutamate receptors put in their place. Nature *386*, 221–222.

Silver, R.A., Cull-Candy, S.G., and Takahashi, T. (1996). Non-NMDA glutamate receptor occupancy and open probability at a rat cerebellar synapse with single and multiple release sites. J. Physiol. (Lond.) *494*, 231–250.

Soltesz, I., and Mody, I. (1994). Patch-clamp recordings reveal powerful GABAergic inhibition in dentate hilar neurons. J. Neurosci. *14*, 2365–2375.

Soltesz, I., Smetters, D.K., and Mody, I. (1995). Tonic inhibition originates from synapses close to the soma. Neuron *14*, 1273–1283.

Somogyi, P., and Hodgson, A.J. (1985). Antisera to $\gamma$-aminobutyric acid. III. Demonstration of GABA in Golgi-impregnated neurons and in conventional electron microscopic sections of cat striate cortex. J. Histochem. Cytochem. *33*, 249–257.

Somogyi, P., Fritschy, J.-M., Benke, D., Roberts, J.D.B., and Sieghart, W. (1996). The $\gamma$2 subunit of the $GABA_A$ receptor is concentrated in synaptic junctions containing the $\alpha$1 and $\beta$2/3 subunits in hippocampus, cerebellum and globus pallidus. Neuropharmacology *35*, 1425–1444.

Sur, C., Triller, A., and Korn, H. (1995). Morphology of the release site of inhibitory synapses on the soma and dendrite of an identified neuron. J. Comp. Neurol. *351*, 247–260.

Tong, G., and Jahr, C.E. (1994a). Multivesicular release from excitatory synapses of cultured hippocampal neurons. Neuron *12*, 51–59.

Tong, G., and Jahr, C.E. (1994b). Block of glutamate transporters potentiates postsynaptic excitation. Neuron *13*, 1195–1203.

Traynelis, S.F., Silver, R.A., and Cull-Candy, S.G. (1993). Estimated conductance of glutamate receptor channels activated during EPSCs at the cerebellar mossy fiber-granule cell synapses. Neuron *11*, 279–289.

Tretter, V., Ehya, N., Fuchs, K., and Sieghart, W. (1997). Stoichiometry and assembly of a recombinant $GABA_A$ receptor subtype. J. Neurosci. *17*, 2728–2723.

Triller, A., Cluzeaud, F., Pfeiffer, F., Betz, H., and Korn, H. (1985). Distribution of glycine receptors at central synapses: an immunoelectron microscopy study. J. Cell Biol. *101*, 683–688.

Vicini, S., Alho, H., Costa, E., Mienville, J.M., Santi, M.R., and Vaccarino, F.M. (1986). Modulation of gamma-aminobutyric acid-mediated inhibitory synaptic currents in dissociated cortical cell cultures. Proc. Natl. Acad. Sci. USA *83*, 9269–9273.

Walmsley, B. (1995). Interpretation of 'quantal' peaks in distributions of evoked synaptic transmission at central synapses. Proc. R. Soc. Lond. [Biol.] *261*, 245–250.

Zezula, J., Fuchs, K., and Sieghart, W. (1991). Separation of $\alpha$1, $\alpha$2 and $\alpha$3 subunits of the $GABA_A$-benzodiazepine receptor complex by immunoaffinity chromatography. Brain Res. *563*, 325–328.

Zhang, L., Weiner, J.L., and Carlen, P.L. (1993). Potentiation of $\gamma$-aminobutyric acid type A receptor-mediated synaptic currents by pentobarbital and diazepam in immature hippocampal CA1 neurons. J. Pharmacol. Exp. Ther. *266*, 1227–1235.